

# Bidirectional rectifier with gate voltage control based on $\text{Bi}_2\text{O}_2\text{Se}/\text{WSe}_2$ heterojunction

Ruonan Li<sup>1</sup>, Fangchao Lu<sup>1</sup>, Jiajun Deng<sup>1</sup>, Xingqiu Fu<sup>1</sup>, Wenjie Wang<sup>1,†</sup>, and He Tian<sup>2,†</sup>

<sup>1</sup>North China Electric Power University and Hebei Key Laboratory of Physics and Energy Technology, Beijing 102206, China

<sup>2</sup>School of Integrated Circuits & Beijing National Research on Information Science and Technology (BNRist), Tsinghua University, Beijing 100084, China

**Abstract:** Two-dimensional (2D)  $\text{WSe}_2$  has received increasing attention due to its unique optical properties and bipolar behavior. Several  $\text{WSe}_2$ -based heterojunctions exhibit bidirectional rectification characteristics, but most devices have a lower rectification ratio. In this work, the  $\text{Bi}_2\text{O}_2\text{Se}/\text{WSe}_2$  heterojunction prepared by us has a type II band alignment, which can vastly suppress the channel current through the interface barrier so that the  $\text{Bi}_2\text{O}_2\text{Se}/\text{WSe}_2$  heterojunction device has a large rectification ratio of about  $10^5$ . Meanwhile, under different gate voltage modulation, the current on/off ratio of the device changes by nearly five orders of magnitude, and the maximum current on/off ratio is expected to be achieved  $10^6$ . The photocurrent measurement reveals the behavior of recombination and space charge confinement, further verifying the bidirectional rectification behavior of heterojunctions, and it also exhibits excellent performance in light response. In the future,  $\text{Bi}_2\text{O}_2\text{Se}/\text{WSe}_2$  heterojunction field-effect transistors have great potential to reduce the volume of integrated circuits as a bidirectional controlled switching device.

**Key words:**  $\text{Bi}_2\text{O}_2\text{Se}$ ;  $\text{WSe}_2$ ; heterojunction; bidirectional rectification; optoelectronic devices

**Citation:** R N Li, F C Lu, J J Deng, X Q Fu, W J Wang, and H Tian, Bidirectional rectifier with gate voltage control based on  $\text{Bi}_2\text{O}_2\text{Se}/\text{WSe}_2$  heterojunction[J]. *J. Semicond.*, 2024, 45(1), 012701. <https://doi.org/10.1088/1674-4926/45/1/012701>

## 1. Introduction

Since the discovery of graphene, a variety of two-dimensional layered van der Waals (vdW) materials have been synthesized and their unique and attractive physical properties have been reported<sup>[1–3]</sup>. Due to the absence of suspension keys on the surface, van der Waals heterojunctions do not require strict lattice matching, so they can be combined flexibly and conveniently, opening up more possibilities for transistor performance optimization and function development. Conventional heterojunction transistors have diode rectification characteristics that allow only a single direction of current to pass between the heterojunction regions. At present, the more popular bidirectional rectifier diode is composed of two pn junction diodes, when a voltage is applied to one of the pn junctions, the junction is in the conduction state, and the other is in the cut-off state, and vice versa, so that the current can be turned on in both positive and negative directions, to achieve the effect of bidirectional rectification. Therefore, bidirectional rectifier diodes are extensively applied to the control of reversible DC motors, converters, inverters, and other fields<sup>[4]</sup>. Compared with unidirectional rectifier diodes, bidirectional rectifier diodes have better efficiency, faster response speed, and a wider range of application scenarios. However, due to the need for two diode combinations, it is difficult to break through the size reduction of large-scale integration.

Therefore, researching the bidirectional rectification characteristics of individual heterojunctions will pave the way for the size reduction of integrated circuits. As a bipolar semiconductor material<sup>[5]</sup>,  $\text{WSe}_2$  can be adjusted by gate voltage to control its carrier concentration and doping amount, to exhibit different polarities<sup>[6, 7]</sup>. At present, the bidirectional rectification behavior of  $\text{WSe}_2$ -based heterojunction has arisen<sup>[8–10]</sup>. In the  $\text{WSe}_2/\text{GeSe}$  heterojunction, the  $\text{WSe}_2$  Fermi level can be regulated over the entire bandgap range by adjusting the external gate voltage, and bidirectional rectification is implemented<sup>[11]</sup>. Generally, the reverse leakage current increases due to the minority carriers during reverse bias, resulting in a low rectification ratio<sup>[12]</sup>. However, the type II band structure can suppress the leakage current through the interface barrier, to achieve a high rectification ratio<sup>[13]</sup>.  $\text{Bi}_2\text{O}_2\text{Se}$  material not only forms a type II band alignment with  $\text{WSe}_2$  but also has attracted extensive attention because of its ultra-high mobility. In the  $\text{Bi}_2\text{O}_2\text{Se}$  and  $\text{WSe}_2$  heterojunctions, the carriers on the side of the  $\text{Bi}_2\text{O}_2\text{Se}$  with high mobility are cycled several times to generate gain, thereby improving the photoelectric responsivity. At the same time, as long as the  $\text{Bi}_2\text{O}_2\text{Se}/\text{WSe}_2$  junction is very sharp and there is no additional oxide layer, the photoelectric response speed can rise substantially.

In this work, we fabricated a  $\text{WSe}_2/\text{Bi}_2\text{O}_2\text{Se}$  multilayer vdW heterojunction transistor on a silicon substrate by manual stacking. Fig. 1(a) shows a schematic diagram of the atomic arrangement of the  $\text{Bi}_2\text{O}_2\text{Se}/\text{WSe}_2$  FET, with the white frame line pointing to the arrangement of the atoms in the heterojunction region.  $\text{WSe}_2$  is a typical sandwich structure, with the layers connected by van der Waals forces. The bottom

Correspondence to: W J Wang, [wwj2008@ncepu.edu.cn](mailto:wwj2008@ncepu.edu.cn); H Tian, [tianhe88@tsinghua.edu.cn](mailto:tianhe88@tsinghua.edu.cn)

Received 14 NOVEMBER 2023; Revised 29 NOVEMBER 2023.

©2024 Chinese Institute of Electronics

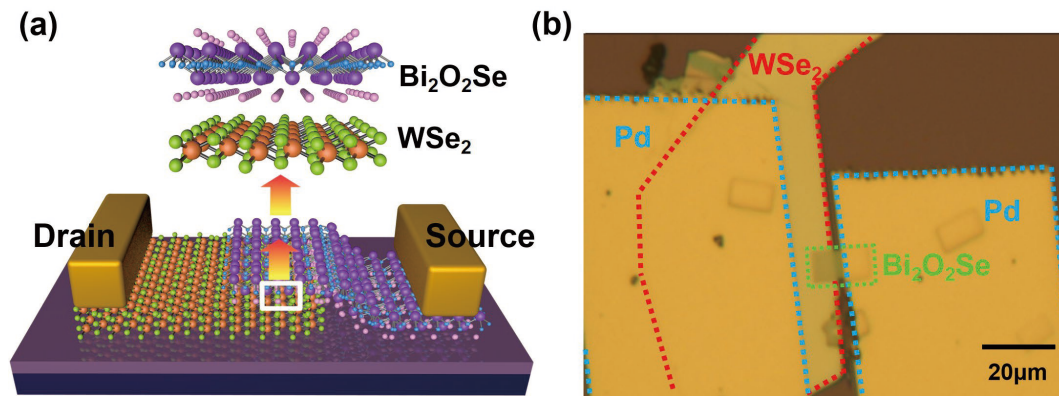


Fig. 1. (Color online) (a) Schematic diagram of  $\text{WSe}_2/\text{Bi}_2\text{O}_2\text{Se}$  FET. (b) Optical micrograph of the  $\text{WSe}_2/\text{Bi}_2\text{O}_2\text{Se}$  FET.

$\text{Bi}_2\text{O}_2\text{Se}$  is alternately distributed in the  $[\text{Se}]_n^{2n-}$  layer and  $[\text{Bi}_2\text{O}_2]_n^{2n+}$  layer, and the  $\text{WSe}_2$  and  $\text{Bi}_2\text{O}_2\text{Se}$  are also combined by weak van der Waals forces.  $\text{Bi}_2\text{O}_2\text{Se}$  has a non-electrically neutral layered structure<sup>[14]</sup>. The electric field that may exist around the material promotes electron–hole separation when the junction is formed, similar to the built-in electric field. The  $\text{Bi}_2\text{O}_2\text{Se}/\text{WSe}_2$  heterojunction transistor we prepared not only has the basic rectification characteristics of diodes, but also can realize the reverse flow of current in the heterojunction region under the control of gate voltage, and has bidirectional rectification characteristics. The rectification ratio ( $I_f/I_r$ ) approaching  $10^5$ . The current on/off ratio of the  $\text{WSe}_2/\text{Bi}_2\text{O}_2\text{Se}$  transistor can be changed by nearly five orders of magnitude under the control of the gate voltage, with the current on/off ratio ( $I_{\text{on}}/I_{\text{off}}$ ) exceeding  $10^5$ . The current on/off ratio is expected to be further improved under the modulation of gate voltage. The photocurrent characterization of the  $\text{WSe}_2/\text{Bi}_2\text{O}_2\text{Se}$  heterostructure verifies the bidirectional switching function of the device. Ultraviolet photoelectron spectroscopy (UPS) proved that the band shift belonged to type II, and the difference in the work function of the two semiconductor materials under Kelvin probe microscopy (KPFM) was completely consistent with the UPS results. We combine the photocurrent test results with the band structure to explain the mechanism of bidirectional regulation of photocurrent by gate–source voltage in heterojunction. In addition, visible light has an excellent spectral response to the near-infrared region, with a maximum photocurrent value of  $176 \mu\text{A}$  and a response time as low as microseconds.

## 2. Method

**Device fabrication** The  $\text{Bi}_2\text{O}_2\text{Se}/\text{WSe}_2$  heterojunction was prepared by the aligned dry transfer method. Tilt-grown  $\text{Bi}_2\text{O}_2\text{Se}$  (30 nm) prepared by chemical vapor deposition on mica substrate is transferred to a clean  $\text{SiO}_2/\text{Si}$  substrate by direct compression<sup>[15]</sup>. Multilayers of  $\text{WSe}_2$  (40 nm) were directly stripped from  $\text{WSe}_2$  bulk materials (2D Semiconductors, China) using mechanical stripping and transferred to polydimethylsiloxane (PDMS) substrates. Observe under the microscope to find suitable  $\text{WSe}_2$  regions and  $\text{Bi}_2\text{O}_2\text{Se}$  for physical marks. Under a 2D transfer system, the PDMS substrate is inverted above the transfer region and the  $\text{SiO}_2/\text{Si}$  substrate with  $\text{Bi}_2\text{O}_2\text{Se}$  is placed below the transfer region. Using a microscope to align the physically labeled area precisely, slowly descend  $\text{WSe}_2$  until it comes into contact with  $\text{Bi}_2\text{O}_2\text{Se}$ , and

slowly raise the PDMS after heating at  $80^\circ\text{C}$  for 10 min, the transfer of the 2D material is completed. Because of the thermal release of polydimethylsiloxane, heating can attenuate the viscosity between  $\text{WSe}_2$  and PDMS, and the  $\text{WSe}_2$  and PDMS are separated after heating due to the van der Waals force between the two 2D materials. We choose the high-function Pd as the contact material to form a larger Schottky junction, thereby reducing the dark current. Metal Pd film is soft and difficult to be transferred by probe under microscope, so we steamed a layer of Au film on the surface of Pd film to facilitate electrode transfer. The Pd/Au electrodes were prepared by vacuum evaporation, the Pd/Au films with thicknesses of 10 nm/100 nm were evaporated sequentially on the  $\text{SiO}_2/\text{Si}$  substrate, and the copper TEM grid was used as a mask to obtain strip Pd/Au electrodes arranged in parallel on the  $\text{SiO}_2/\text{Si}$  substrate. We used probes to transfer the electrodes and build them on either side of the  $\text{Bi}_2\text{O}_2\text{Se}/\text{WSe}_2$  heterojunction. The  $\text{Bi}_2\text{O}_2\text{Se}/\text{WSe}_2$  heterojunction FETs were annealed for 1 h at a vacuum of 8 Pa,  $200^\circ\text{C}$ , and without a carrier gas. The  $\text{Bi}_2\text{O}_2\text{Se}/\text{WSe}_2$  heterojunction optical image is illustrated in Fig. 1(b), with the red border area being  $\text{WSe}_2$ , the green dotted box being  $\text{Bi}_2\text{O}_2\text{Se}$ , and the blue dotted area being the Pd electrode.

**Device characterization** Device electrical curves were obtained using Keysight B1500 SMUs. The surface potential of the sample was measured with an atomic force microscope (AFM, Park) before electrode attachment. The ultraviolet photoelectron spectra of  $\text{Bi}_2\text{O}_2\text{Se}$  and  $\text{WSe}_2$  prepared under the same experimental conditions were collected by UPS (Thermoscalab250X). The photoresponse experiment was performed under 640 nm laser irradiation using a laser spot with a diameter of 1 cm. The response velocity of the  $\text{Bi}_2\text{O}_2\text{Se}/\text{WSe}_2$  heterojunction transistor was measured using a data acquisition card (NI PCIe-6321). The identical sample was used for both the optoelectronic and AFM tests of the device.

## 3. Results and discussion

After the device was fabricated, we tested the electrical performance of the device. Unlike common heterogeneous transistors with diode rectification characteristics<sup>[16]</sup>, Figs. 2(a) and 2(b) show the output curves at gate voltages of 40 V and  $-80$  V, respectively, with an inset of logarithmic coordinates. The  $\text{Bi}_2\text{O}_2\text{Se}/\text{WSe}_2$  heterojunction transistor we prepared exhibits bidirectional rectification under the control of gate voltage. We speculate that when the gate voltage is

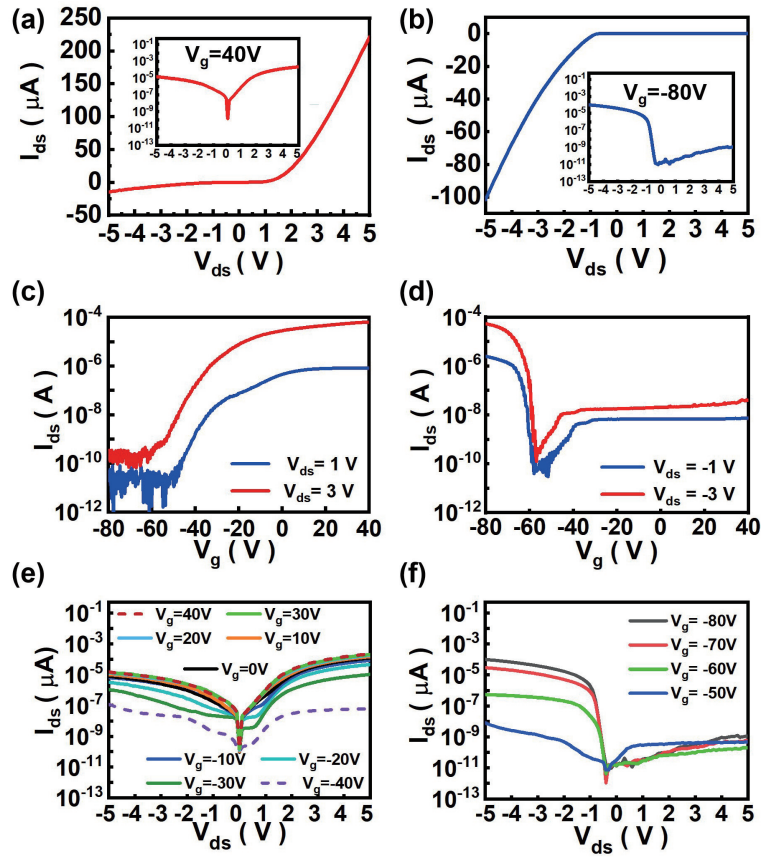


Fig. 2. (Color online) (a) and (b) Output curves at gate voltages of 40 and 80 V with an inset of logarithmic coordinates. (c) and (d) Logarithmic diagram of the transfer curve at different bias voltage  $V_{ds}$ . (e) and (f) Current liner diagram in logarithmic coordinates, recorded by scanning gate voltage  $V_g$ .

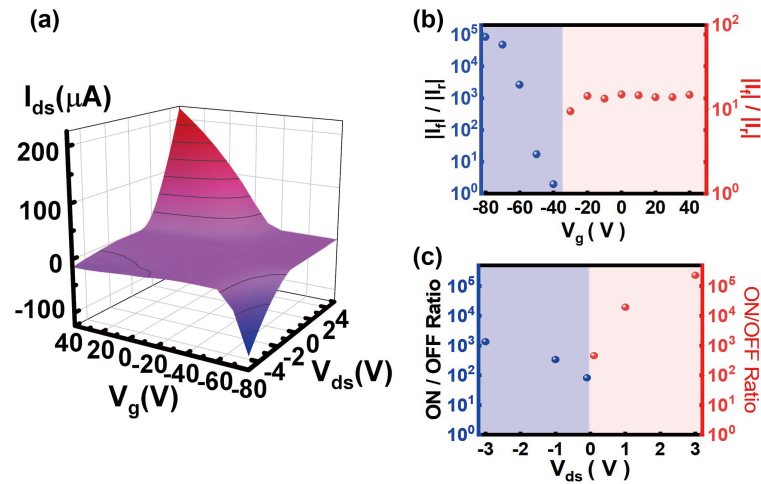


Fig. 3. (Color online) (a) 3D-map of current, recorded by scanning gate voltage  $V_g$  and bias voltage  $V_{ds}$ . (b) The rectifying ratio of the forward current  $I_f$  to the reverse current  $I_r$  at the same gate voltage. (c) On/off ratio of the  $\text{Bi}_2\text{O}_2\text{Se}/\text{WSe}_2$  heterojunction.

changed, the concentration of carriers in the semiconductor material changes accordingly through electrostatic doping, that is, the direction of the built-in electric field formed by the two semiconductor materials is reversed under the action of the gate voltage, so the rectification direction of the heterojunction device is observed. As shown in Figs. 2(c) and 2(d), the logarithmic plot of the transfer curve shows an equally spaced change in gate voltage from  $-80$  to  $40$  V. When the source–drain voltage  $V_{ds} > 0$  V, the gate voltage  $V_g$  is positive, and the heterojunction device is in a conduction state. Conversely, when the source–drain voltage  $V_{ds} < 0$  V and the

gate voltage  $V_g$  is positive, the heterojunction device is in a shutdown state, consistent with our previous measurement output curve. Figs. 2(e) and 2(f) show the logarithmic coordinates of the output curve at different gate voltages from  $-80$  to  $40$  V, showing the forward and reverse rectification, respectively. It can be discovered that between the gate voltage of  $-40$  and  $-30$  V, the direction of rectification changes due to the displacement of the Fermi level in the semiconductor material  $\text{WSe}_2$  by electrostatic doping.

Fig. 3(a) shows the 3D image of the source–drain voltage from  $-5$  to  $5$  V and the gate voltage from  $-80$  to  $40$  V. As

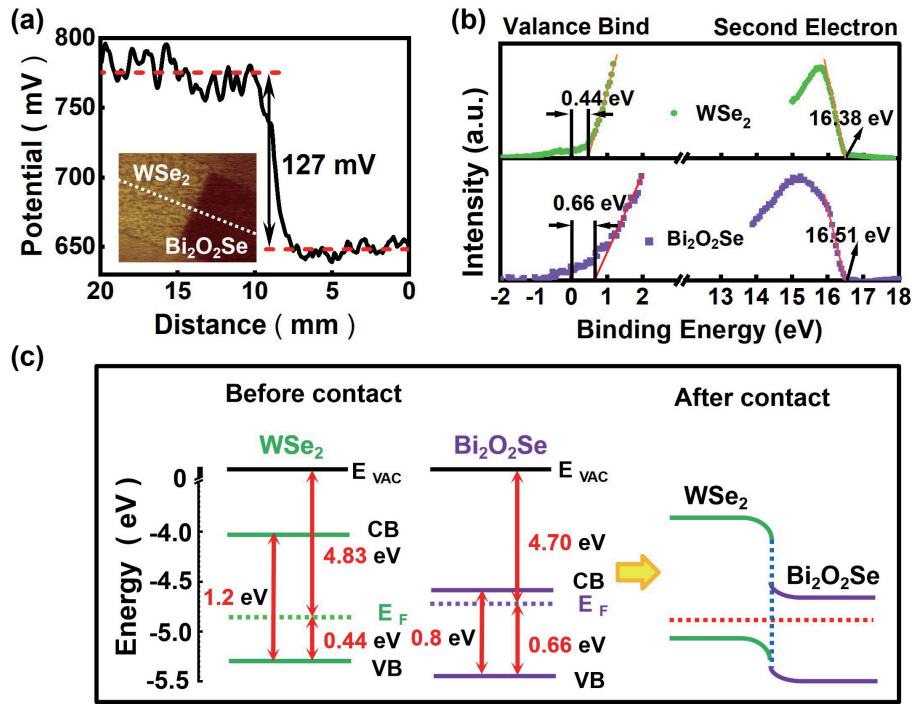


Fig. 4. (Color online) (a) Kelvin Probe Force Microscopy (KPFM) image of the Bi<sub>2</sub>O<sub>2</sub>Se/WSe<sub>2</sub> FET, the inset shows KPFM line scan, denoted by a white dotted line in figure. (b) Ultraviolet photoelectron spectra of WSe<sub>2</sub> and Bi<sub>2</sub>O<sub>2</sub>Se. (c) Band diagrams of the Bi<sub>2</sub>O<sub>2</sub>Se/WSe<sub>2</sub> heterojunction.

can be seen from the figure, the source leakage current is controlled by both the gate voltage and the source leakage voltage, and the Bi<sub>2</sub>O<sub>2</sub>Se/WSe<sub>2</sub> heterojunction transistor exhibits different conductivity due to the change of gate voltage. Fig. 3(b) shows current on/off ratios for the device at source–drain voltages of  $\pm 100$  mV,  $\pm 1$  V, and  $\pm 3$  V, Bi<sub>2</sub>O<sub>2</sub>Se/WSe<sub>2</sub> heterojunction FET current on/off ratio of  $>10^5$  at  $V_g = -80$  V, even at a source–drain voltage of  $\pm 100$  mV, the transistor's current on/off ratio is still greater than  $10^2$ . As shown in Fig. 3(c), the transistor's rectification ratio reaches  $10^5$  at a gate voltage of  $-80$  V and is greater than 10 even at forward bias. If we want to make the circuit conductive in both opposite directions, the simple logic circuit needs to control both transistors at the same time, because conventional diodes can only be single-conductive. But the difference is that we can take advantage of the Bi<sub>2</sub>O<sub>2</sub>Se/WSe<sub>2</sub> heterojunction bidirectional rectification properties and directly use a transistor to control the direction of the current. Diode can be used to achieve triode function, which is expected to be applied to the size reduction of integrated circuits.

The charge transport on the heterostructure is essentially governed by the bands, while the Fermi level is affected by electrostatic doping. We preliminarily determined the relative Fermi level positions between the two semiconductor materials using Kelvin probe force microscopy (KPFM). According to the formula  $W_{\text{Bi}_2\text{O}_2\text{Se}} - W_{\text{WSe}_2} = q(V_{\text{WSe}_2} - V_{\text{Bi}_2\text{O}_2\text{Se}})$ <sup>[17]</sup> (where  $W_{\text{Bi}_2\text{O}_2\text{Se}}$  and  $W_{\text{WSe}_2}$  is the work function of Bi<sub>2</sub>O<sub>2</sub>Se and WSe<sub>2</sub>,  $q$  is the charge of the electron,  $V$  is the surface potential of WSe<sub>2</sub> and Bi<sub>2</sub>O<sub>2</sub>Se). As shown in Fig. 4(a), the difference in work function between the two semiconductor materials is about 127 meV. To obtain a more specific band alignment of the Bi<sub>2</sub>O<sub>2</sub>Se/WSe<sub>2</sub> heterostructure, ultraviolet electron spectroscopy (UPS) was used to test, as shown in Fig. 4(b). The work functions ( $W$ ) of Bi<sub>2</sub>O<sub>2</sub>Se and WSe<sub>2</sub> are calculated to be 4.70 and 4.83 eV, respectively, by subtract-

ing the second electron cut-off energy from the energy of the He I light source (21.21 eV), and the work functions of the two materials are consistent with the test results of KPFM. The distance between the edge of their valence band and the Fermi level is 0.66 and 0.44 eV, respectively. According to the multilayer Bi<sub>2</sub>O<sub>2</sub>Se with a bandgap of 1.2 eV, its electronic affinity is about 4.07 eV<sup>[18, 19]</sup>. Similarly, for bulk WSe<sub>2</sub>, the band gap and electron affinity are about 0.8 and 4.56 eV<sup>[20, 21]</sup>, respectively. The conduction band edge and valence band edge of WSe<sub>2</sub> are 0.49 and 0.09 higher than those of Bi<sub>2</sub>O<sub>2</sub>Se, respectively. Therefore, the band arrangement before and after the contact between Bi<sub>2</sub>O<sub>2</sub>Se and WSe<sub>2</sub> is shown in Fig. 4(c), after the two materials come into contact, electrons flow to the WSe<sub>2</sub> side with a higher work function, and the band bends under the action of the built-in electric field, as shown in the figure on the right.

An unambiguous analysis of the effect of gate voltage on heterojunction devices requires an understanding of band structure variation. The application of gate voltage creates a vertical external electric field on the surface of the semiconductor material, and there is a significant electrostatic potential in the semiconductor. For electrons, a decrease in the electric potential along the direction of the electric field means that the potential energy increases, the energy level of the electron increases, and the energy band bends accordingly. Therefore, we tried to characterize the electrostatic potential distribution in semiconductors by photocurrent mapping to find the correlation. Carrier concentration in the raw material is estimated according to  $p_{\text{WSe}_2} (n_{\text{Bi}_2\text{O}_2\text{Se}}) = C_g |V_{\text{th}}| / q$ , where electron charge  $q = 1.6 \times 10^{-19}$  C, the capacitance of 275 nm SiO<sub>2</sub>  $C_g = \epsilon_0 \epsilon_r / d = 1.26 \times 10^{-8}$  F · cm<sup>-2</sup>, the vacuum dielectric constant  $\epsilon_0 = 8.85 \times 10^{-12}$  F · m<sup>-2</sup>, the relative dielectric constant of 275-nm SiO<sub>2</sub>  $\epsilon_r = 3.9$ <sup>[22]</sup>. Supplement Fig. S1 shows the threshold voltages  $V_{\text{th}}$  of  $-25.13$  and  $-32.46$  V for WSe<sub>2</sub> and Bi<sub>2</sub>O<sub>2</sub>Se, respectively. Then the carrier concentrations of WSe<sub>2</sub>



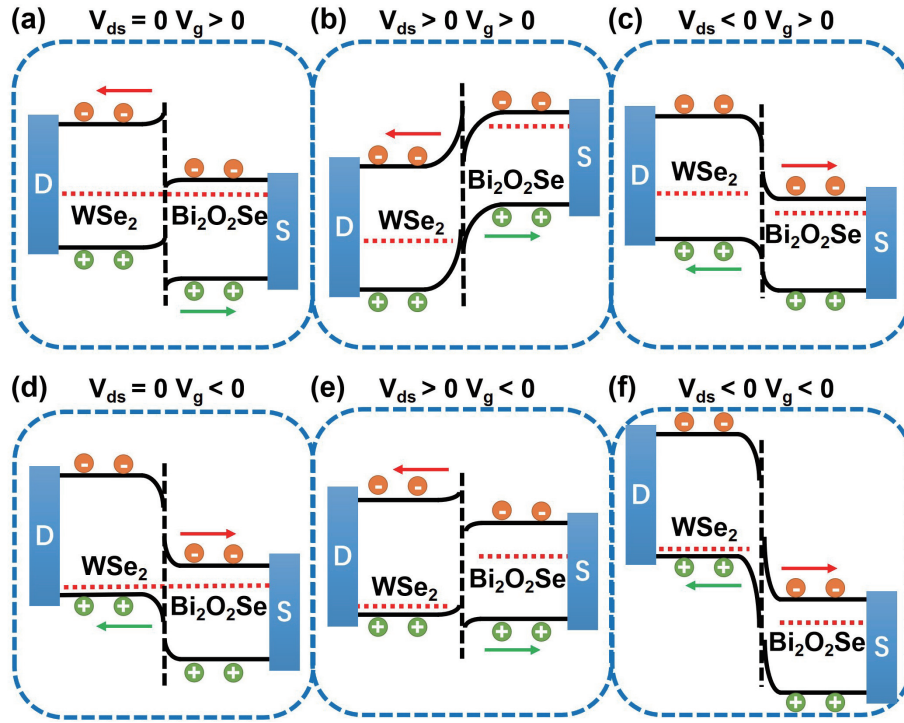


Fig. 5. (Color online) Band diagrams of the junction with photoexcitation under the different  $V_{ds}$  and  $V_g$ , which reflected the charge transport process.

and  $\text{Bi}_2\text{O}_2\text{Se}$  are  $1.97 \times 10^{12}$  and  $2.56 \times 10^{12} \text{ cm}^{-2}$ , respectively. Lower carrier concentration of  $\text{WSe}_2$  than  $\text{Bi}_2\text{O}_2\text{Se}$ , coupled with direct contact between  $\text{WSe}_2$  and the substrate indicate that the influence of  $\text{WSe}_2$  Fermi energy level is more obvious in the process of electrostatic doping. The conduction band and valence band are still discontinuous, intensifying the band bending.

In the pn junction, the uneven distribution of carrier concentrations in the two materials leads to a directional shift of the carriers from the place of high concentration to the area of low concentration. The electrons in  $\text{Bi}_2\text{O}_2\text{Se}$  move to the  $\text{WSe}_2$  side, leaving immovable positive-charged ionized donors who lose their equilibrium negative charge and thus form a positive charge area on the N side near the pn junction. Similarly, a negatively charged area consisting of ionized acceptors appears on the side of the p-region near the pn junction. These charges in the space charge region generate a built-in electric field pointing from the  $\text{Bi}_2\text{O}_2\text{Se}$  side towards  $\text{WSe}_2$ . In the absence of external source–drain voltage and gate voltage, photogenerated electron–hole pairs are generated on the surface of  $\text{Bi}_2\text{O}_2\text{Se}$  by 640 nm monochromatic excitation. Recombination occurs when they do not separate into the junction region. Due to the presence of in-plane heterojunctions between  $\text{WSe}_2$  near the junction and  $\text{WSe}_2$  away from the junction, photocurrents appear around the junction region rather than in the upper layer. Under the internal electric field, the electrons move to the side of  $\text{Bi}_2\text{O}_2\text{Se}$ , and the holes move to the side of  $\text{WSe}_2$ , forming a photocurrent from  $\text{Bi}_2\text{O}_2\text{Se}$  to  $\text{WSe}_2$ .

If a positive gate voltage ( $\text{Bi}_2\text{O}_2\text{Se}$  to  $\text{WSe}_2$ ) is applied, the gate injects electrons through the gate medium into the heterojunction. The potential energy of the electrons in the conduction band and valence band decreases overall, resulting in a downward shift of the conduction band and valence

band relative to the Fermi level. If the  $V_g$  is high enough to provide a large enough electric field, the direction of the electric field can be changed, which is described in Fig. 5(a) for this extreme condition. If a positive source–drain voltage ( $V_{ds}$ ) is added to the positive  $V_g$ , the potential energy on the  $\text{Bi}_2\text{O}_2\text{Se}$  side will increase, causing the energy band to shift upward, as shown in Fig. 5(b). If enough positive bias is added, the energy of the electrons in the junction will be higher than the barrier energy. In other words, electrons are more likely to cross the barrier to reach the  $\text{WSe}_2$  side, and the higher the gate voltage, the more likely they are to jump. Under the superposition of  $V_g$  and  $V_{ds}$ , the direction of the total electric field is from  $\text{WSe}_2$  to  $\text{Bi}_2\text{O}_2\text{Se}$ . At this time, photogenerated carriers are generated in the material by the excitation beam. Under the action of the applied electric field, the holes excited by the light migrate from  $\text{WSe}_2$  to the source, and the electrons in  $\text{Bi}_2\text{O}_2\text{Se}$  diffuse to the drain. As a result, the photocurrents from  $\text{WSe}_2$  to  $\text{Bi}_2\text{O}_2\text{Se}$  are in the Fig. 6(c). Fig. 6(a) shows the photocurrent scan area, and Fig. 6(b) shows zero gate voltage and source–drain voltage. As shown in Fig. 5(c), when  $V_{ds} < 0$ , the opposite direction of the electric field causes the light-generated carriers to migrate in the opposite direction. The carrier concentration is low, the photocurrent is weak, and the photocurrent pattern corresponds to Fig. 6(d).

In the case of a negative gate voltage, the band shifts upwards concerning the Fermi level as a whole, as shown in Fig. 5(d). In Fig. 5(e), the electron energy on the  $\text{Bi}_2\text{O}_2\text{Se}$  side decreases at  $V_{ds} > 0$  compared to the  $V_g > 0$  time, and the potential barrier increases, making it difficult for the electrons to transition. In this case, the  $I$ – $V$  curve appears to be turned off and a pulsed photocurrent appears, as shown in Fig. 6(e). When the source–leakage voltage  $V_{ds}$  is negative, a large total electric field is obtained by superimposing  $V_g$  and

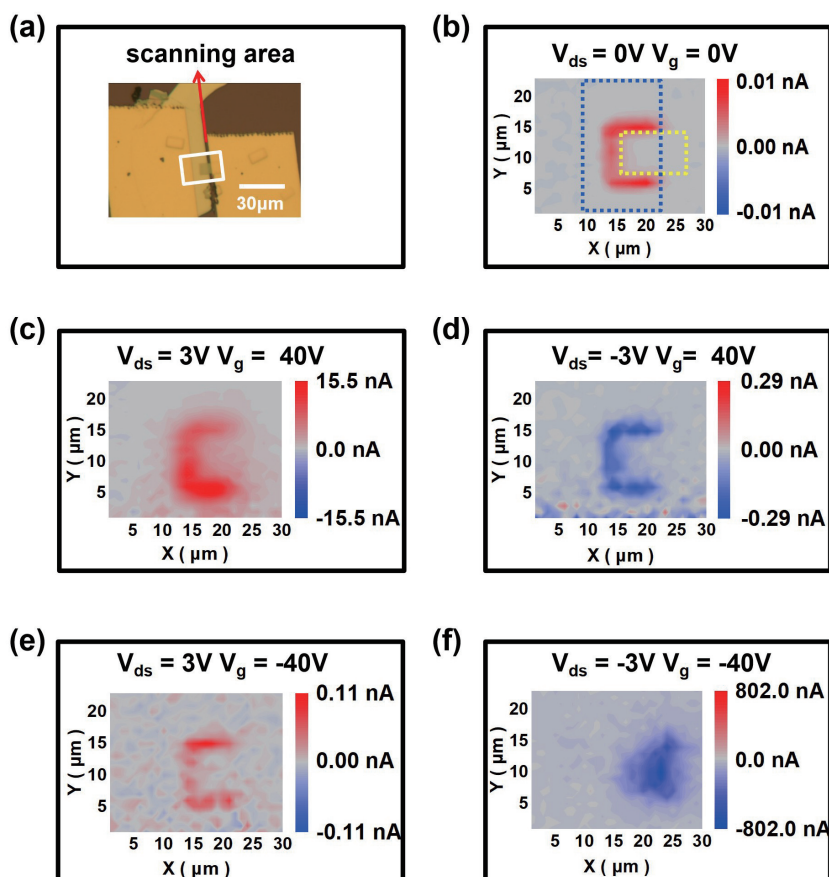


Fig. 6. (Color online) Photocurrent map of the  $\text{Bi}_2\text{O}_2\text{Se}/\text{WSe}_2$  heterojunction field-effect transistor. (a)  $\text{Bi}_2\text{O}_2\text{Se}/\text{WSe}_2$  heterojunction optical images, the white box indicates scanning area; (b)  $V_{ds} = 0 \text{ V}$ ,  $V_g = 0 \text{ V}$ ; (c)  $V_{ds} = 3 \text{ V}$ ,  $V_g = 40 \text{ V}$ ; (d)  $V_g = -3 \text{ V}$ ,  $V_{ds} = 40 \text{ V}$ ; (e)  $V_{ds} = 3 \text{ V}$ ,  $V_g = -40 \text{ V}$ ; (f)  $V_{ds} = -3 \text{ V}$ ,  $V_g = -40 \text{ V}$ .

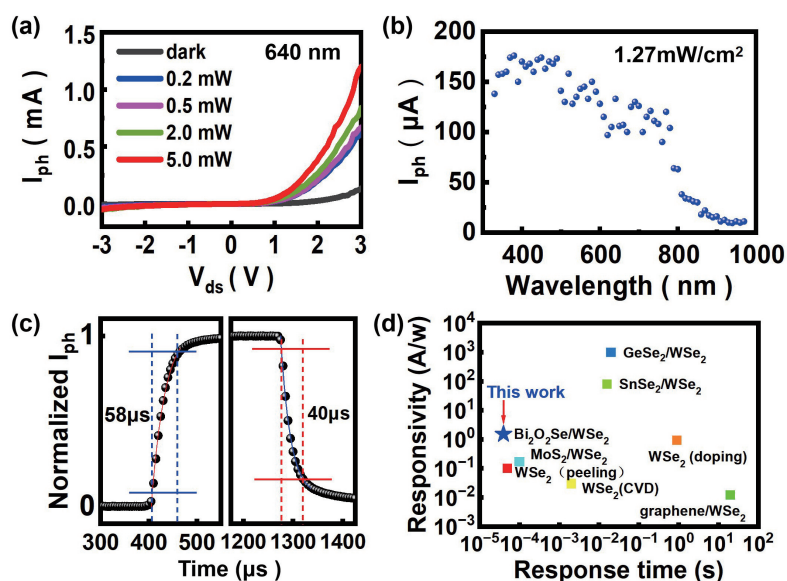


Fig. 7. (Color online) (a) Output curves of  $\text{Bi}_2\text{O}_2\text{Se}/\text{WSe}_2$  heterojunctions under different light power irradiation. (b) Spectral response of the heterojunctions. (c) Response time of the device over one response cycle. (d) Composite comparison diagram of photoresponse performance among  $\text{WSe}_2$ -based photodetectors<sup>[11, 23–28]</sup>.

$V_{ds}$  in the same direction as the built-in electric field, resulting in severe band bending and a very narrow barrier, which may lead to direct tunneling, as shown in Fig. 5(f). As a result, the  $\text{Bi}_2\text{O}_2\text{Se}/\text{WSe}_2$  heterojunction FETs are in a conductive state and the photocurrent is significantly increased, as shown in Fig. 6(f). Under illumination, the difference in work

function between  $\text{Bi}_2\text{O}_2\text{Se}$  and  $\text{WSe}_2$  leads to the formation of an built-in electric field between  $\text{Bi}_2\text{O}_2\text{Se}$  and  $\text{WSe}_2$ , and the presence of the built-in electric field is conducive to the separation of electrons and holes so that the heterojunction region has a powerful light intensity. Compared with horizontal heterojunctions, the photocurrents generated by vertical hetero-

junctions are not obvious, which is due to the absorption of light by the thicker  $\text{Bi}_2\text{O}_2\text{Se}$  in the junction region. However, in the case of the tunneling effect, the photocurrent is so strong that it covers the entire junction region.

When 640 nm monochromatic light irradiates the surface of the heterojunction,  $\text{Bi}_2\text{O}_2\text{Se}$  and  $\text{WSe}_2$  are excited to form electron–hole pairs, which effectively separate under the action of the built-in electric field. And move in different directions to generate photocurrent. As the light intensity increases, the photocurrent in the transistor increases, as shown in Fig. 7(a). Due to the narrow bandgap of  $\text{Bi}_2\text{O}_2\text{Se}$  and the wide bandgap of  $\text{WSe}_2$ , the optical response range of the  $\text{Bi}_2\text{O}_2\text{Se}/\text{WSe}_2$  heterojunction FET in Fig. 7(b) can cover the visible near-infrared region. Under monochromatic excitation at a wavelength of 380 nm, the maximum photocurrent value can reach  $176 \mu\text{A}$ . Even in the near-infrared region, where the response is minimal, the photocurrent value can attain  $11 \mu\text{A}$ . Meanwhile, it also confirms the analysis above, that the photocurrent is mainly contributed by the light absorption on the side of  $\text{WSe}_2$ , and then the photogenerated carriers are separated in the junction region. If  $\text{Bi}_2\text{O}_2\text{Se}$  is the main contribution, the response range can be extended to about  $1550 \text{ nm}$ <sup>[14]</sup>. The switching characteristics of the photocurrent of the device are in Fig. 7(c). At a wavelength of 640 nm and a power density of  $1.27 \text{ mW}/\text{cm}^2$ . The switching characteristics of the transistor are evident, with rise and fall times of 58 and  $40 \mu\text{s}$ , respectively. The rise time is generally defined as the time to rise from 10% to 90% of the waveform, and the fall time is reversed. The recombination rate of the carriers is faster than the rate of generation, which we attribute to the inherent defects of the material.  $\text{Bi}_2\text{O}_2\text{Se}/\text{WSe}_2$  heterojunction generates photogenerated carriers in the junction region, and then the electrons and holes are separated until they are combined in the outer circuit, thus completing a photoelectric response. Due to the high mobility of  $\text{Bi}_2\text{O}_2\text{Se}$ , multiple carrier cycles on the  $\text{Bi}_2\text{O}_2\text{Se}$  side produce a gain, the device has a high responsivity of about  $1500 \text{ mA}/\text{W}$ . The  $\text{Bi}_2\text{O}_2\text{Se}/\text{WSe}_2$  heterojunction transistors have an advantage in terms of comprehensive performance in response time and responsivity, both when compared to  $\text{WSe}_2$  transistors prepared in different ways<sup>[23–25]</sup>, and when compared to other  $\text{WSe}_2$ -based heterojunction transistors previously reported<sup>[11, 26–28]</sup>. In addition, the detectivity of our device can reach  $1.65 \times 10^7$  jones. Our results demonstrate the potential of  $\text{Bi}_2\text{O}_2\text{Se}/\text{WSe}_2$  heterojunction FET in the fields of bidirectional rectification and fast response.

#### 4. Conclusion

In summary, we accurately aligned the multilayer  $\text{WSe}_2$  crystals prepared by mechanical exfoliation with  $\text{Bi}_2\text{O}_2\text{Se}$  grown by chemical vapor deposition to construct the  $\text{Bi}_2\text{O}_2\text{Se}/\text{WSe}_2$  heterojunction FET, which not only exhibits basic diode characteristics but can also be back-biased under the control of gate voltage, the rectification ratio of the device can approach  $10^5$ . Under different gate voltage modulation, the current on/off ratio of the device changes by nearly five orders of magnitude, meanwhile the maximum current on/off ratio of the device has outdistanced  $10^5$ . The work functions and band alignment obtained by KPFM and UPS are consistent with type II heterojunction characteristics. The conjec-

ture that the direction of the electric field in the heterojunction depends on the inversion of the gate voltage is verified by the interpretation of the photocurrent diagram. The on/off of the device is controlled by adjusting the gate voltage and the source–drain voltage, and the related mechanisms are described in detail. In addition, the device has excellent optoelectronic characteristics, with a spectral response from visible light to the near-infrared region, and the rise and fall times of the light response in the order of microseconds within a single light response cycle. Therefore, the device has a gate voltage regulation function and unique optoelectronic characteristics, which is expected to broaden the application of two-dimensional material heterojunction devices in the field of optoelectronics, and take a significant step for the development of high-performance bidirectional rectifiers concurrently.

#### Acknowledgements

This work was supported by the National Natural Science Foundation of China (61704054, 92161115, 62374099, and 62022047), the Fundamental Research Funds for the Central Universities (JB2020MS042 and JB2019MS051).

#### Appendix A. Supplementary material

Supplementary materials to this article can be found online at <https://doi.org/10.1088/1674-4926/45/1/012701>.

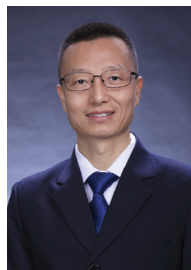
#### References

- [1] Cheng R, Li D H, Zhou H L, et al. Electroluminescence and photocurrent generation from atomically sharp  $\text{WSe}_2/\text{MoS}_2$  heterojunction p–n diodes. *Nano Letters*, 2014, 14(10), 5590
- [2] Xiao J W, Zhang Y, Chen H J, et al. Enhanced performance of a monolayer  $\text{MoS}_2/\text{WSe}_2$  heterojunction as a photoelectrochemical cathode. *Nano-Micro Letters*, 2018, 10(4), 60
- [3] Deng Y X, Luo Z, Conrad N J, et al. Black phosphorus–monolayer  $\text{MoS}_2$  van der waals heterojunction p–n diode. *ACS Nano*, 2014, 8(8), 8292
- [4] Deng J Q, Cheng H, Wang C, et al. Evaluation and comprehensive comparison of H-bridge-based bidirectional rectifier and unidirectional rectifiers. *Electronics*, 2020, 9, 309
- [5] Wang Z G, Li Q, Chen Y F, et al. The ambipolar transport behavior of  $\text{WSe}_2$  transistors and its analogue circuits. *NPG Asia Mater*, 2018, 10(8), 703
- [6] Wu F, Li Q, Wang P, et al. High efficiency and fast van der Waals hetero-photodiodes with a unilateral depletion region. *Nat Commun*, 2019, 10(1), 4663
- [7] Pudasaini P R, Stanford M G, Oyedele A, et al. High performance top-gated multilayer  $\text{WSe}_2$  field effect transistors. *Nanotechnology*, 2017, 28(47), 475202
- [8] Xiao S D, Li M D, Seabaugh A, et al. Vertical heterojunction of  $\text{MoS}_2$  and  $\text{WSe}_2$ . *72nd Device Research Conference, Santa Barbara, CA, USA, 2014*
- [9] Patel A B, Chauhan P, Patel K, et al. Solution-processed uniform  $\text{MoSe}_2$ – $\text{WSe}_2$  heterojunction thin film on silicon substrate for superior and tunable photodetection. *ACS Sustainable Chem Eng*, 2020, 8(12), 4809
- [10] Abderrahmane A, Woo C, Jung P G, et al. Multifunctional  $\text{WSe}_2/\text{MoSe}_2/\text{WSe}_2/\text{MoSe}_2$  heterostructures. *Mater Sci Semicond Process*, 2024, 169, 107864
- [11] Yang Z Y, Liao L, Gong F, et al.  $\text{WSe}_2/\text{GeSe}$  heterojunction photodiode with giant gate tunability. *Nano Energy*, 2018, 49, 103
- [12] Aftab S, Samiya, Ul Haq H M, et al. Van der waals multi-hetero-

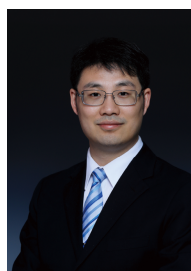
- structures (PN, PIN, and NPN) for dynamic rectification in 2D materials. *Adv Materials Inter*, 2020, 7(24), 2001479
- [13] Zhou X, Hu X, Yu J, et al. 2D layered material - based van der Waals heterostructures for optoelectronics. *Advanced Functional Materials*, 2018, 28(14), 1706587
- [14] Tong T, Chen Y F, Qin S C, et al. Sensitive and ultrabroadband phototransistor based on two-dimensional Bi<sub>2</sub>O<sub>2</sub>Se nanosheets. *Adv Funct Materials*, 2019, 29, 1905806
- [15] Hong C Y, Huang G F, Yao W W, et al. Thickness-modulated in-plane Bi<sub>2</sub>O<sub>2</sub>Se homojunctions for ultrafast high-performance photodetectors. *Chin Phys B*, 2019, 28, 128502
- [16] Wang Q S, Wen Y, Cai K M, et al. Nonvolatile infrared memory in MoS<sub>2</sub>/PbS van der Waals heterostructures. *Sci Adv*, 2018, 4, eaap7916
- [17] Zhou X, Hu X Z, Zhou S S, et al. Tunneling diode based on WSe<sub>2</sub>/SnS<sub>2</sub> heterostructure incorporating high detectivity and responsivity. *Adv Mater*, 2018, 30, 1703286
- [18] Luo P, Zhuge F W, Wang F K, et al. PbSe quantum dots sensitized high-mobility Bi<sub>2</sub>O<sub>2</sub>Se nanosheets for high-performance and broadband photodetection beyond 2 μm. *ACS Nano*, 2019, 13, 9028
- [19] Wu J X, Yuan H T, Meng M M, et al. High electron mobility and quantum oscillations in non-encapsulated ultrathin semiconducting Bi<sub>2</sub>O<sub>2</sub>Se. *Nat Nanotechnol*, 2017, 12, 530
- [20] Doan M H, Jin Y, Adhikari S, et al. Charge transport in MoS<sub>2</sub>/WSe<sub>2</sub> van der waals heterostructure with tunable inversion layer. *ACS Nano*, 2017, 11, 3832
- [21] Kang W M, Cho I T, Roh J, et al. High-gain complementary metal-oxide-semiconductor inverter based on multi-layer WSe<sub>2</sub> field effect transistors without doping. *Semicond Sci Technol*, 2016, 31(10), 105001
- [22] Fan S D, Yun S J, Yu W J, et al. Tailoring quantum tunneling in a vanadium-doped WSe<sub>2</sub>/SnSe<sub>2</sub> heterostructure. *Adv Sci*, 2020, 7(3), 1902751
- [23] Luo M, Wu F, Long M S, et al. WSe<sub>2</sub>/Au vertical Schottky junction photodetector with low dark current and fast photoresponse. *Nanotechnology*, 2018, 29, 444001
- [24] Zheng Z Q, Zhang T M, Yao J, et al. Flexible, transparent and ultra-broadband photodetector based on large-area WSe<sub>2</sub> film for wearable devices. *Nanotechnology*, 2016, 27, 225501
- [25] Sun M X, Xie D, Sun Y L, et al. Locally hydrazine doped WSe<sub>2</sub> p-n junction toward high-performance photodetectors. *Nanotechnology*, 2018, 29, 015203
- [26] Xue H, Dai Y Y, Kim W, et al. High photoresponsivity and broadband photodetection with a band-engineered WSe<sub>2</sub>/SnSe<sub>2</sub> heterostructure. *Nanoscale*, 2019, 11, 3240
- [27] Xu H, Han X Y, Dai X A, et al. High detectivity and transparent few-layer MoS<sub>2</sub>/glassy-graphene heterostructure photodetectors. *Adv Mater*, 2018, 30, 1706561
- [28] Lee H S, Ahn J, Shim W, et al. 2D WSe<sub>2</sub>/MoS<sub>2</sub> van der Waals heterojunction photodiode for visible-near infrared broadband detection. *Appl Phys Lett*, 2018, 113, 163102



**Ruonan Li** got her bachelor's degree in 2020 from BeiHua University and her master's degree in 2023 from North China Electric Power University. Her research focuses on the growth of 2D transition metal chalcogenides and device preparation.



**Wenjie Wang** now works at North China Electric Power University and received his Ph.D. in condensed matter physics from the Superlattice Laboratory of the Institute of Semiconductors, Chinese Academy of Sciences in 2007. His current research interests include growth of two-dimensional materials, photoelectric properties and first-principles computation.



**He Tian** received the Ph.D. degree from the Institute of Microelectronics, Tsinghua University, Beijing, China, in 2015. He is currently an Associate Professor with Tsinghua University. He has co-authored over 200 papers and more than 8000 citations. His current research interests include various 2-D material-based novel nanodevices.